Proceedings of the ASME 2013 Rail Transportation Division Fall Technical Conference
RTDF2013
October 15-17, 2013, Altoona, Pennsylvania, USA

RTDF2013-4705

Towards a Better Understanding of the Rail Grinding Mechanism

Shaodan Zhi
PhD student: Beijing Jiaotong University, Beijing, China

Dr. Allan M. Zarembski PE, FASME Hon. Mbr. AREMA
Research Professor and Director of Railroad Engineering Program, University of Delaware, Newark, Delaware USA

Dr. Jianyong Li
Dean, Professor, Beijing Jiaotong University, Beijing, China

ABSTRACT

Rail grinding continues to be one of the most effective techniques for extending rail life, improving wheel/rail contact behavior, and reducing the overall cost of track maintenance. While the ability to more effectively implement improved rail grinding programs continues to expand, the understanding of the grinding mechanism itself has not kept pace with the improved implementation. Thus, while railroad engineering and maintenance personnel have learned to better develop grinding patterns and profiles through empirical testing and field evaluation, the fundamental theoretical bases for the improved grinding performance have not kept pace.

One such fundamental area of understanding is the modeling of the rail grinding process itself, both individually, as a function of a single grinding motor on the head of the rail, and in the more complex configuration of multiple grinding motors in a range of patterns. This paper presents the results of research directly aimed at better understanding these mechanisms and then utilizing this better understanding to develop a detailed rail grinding model that allows for the accurate analysis of not only an individual grinding motor but also a full grinding train application, as a function of pattern and speed.

In the case of the single grinding motor on the head of the rail, this research looks at the fundamental mechanism associated with each cutting abrasive grinding grain in the grinding stone, and then expands that mechanism to a full 10 inch diameter grinding wheel as it cuts into the rail head at a defined angle and speed. Using actual rail profile data and grinding data, a theoretical grinding wheel model is developed and then calibrated with wheel test data and actual grinding (field) data.

This single motor model is then expanded into a full grinding train model, such as for a 96 stone grinding train with 48 motors per rail, where it is able to analyze the full sequence of 48 motors as each motor individually and sequentially removes metal from the rail head. The resulting analysis is sensitive to such key factors as grinding speed, and the key pattern parameters of motor angles, sequence and power. The model is then calibrated to and compared with actual full scale rail grinding metal removal data from a major Class 1 railroad.

Such an analysis tool allows railroads to analyze the performance of different grinding patterns in a real world operating setting, to improve their rail grinding practices and take further advantage of new technologies in rail grinding to better manage the grinding process and improve planning of grinding activities.

INTRODUCTION

Rail represents one of the most critical and expensive parts of the railroad track infrastructure and one that is subject to significant levels of loading and stress. As such, its maintenance is of serious importance to railroad engineering and track maintenance departments. However, the specific types of maintenance available for addressing rail problems, other than simply replacing the rail, are limited. In the area of rail fatigue and surface defects, rail grinding is and continues to be one of the most effective techniques for extending rail life, improving wheel/rail contact behavior, and reducing the overall cost of track maintenance. From a practical implementation perspective, the ability to more effectively implement improved rail grinding programs continues to expand. This includes better

understanding of the wheel/rail interaction mechanism that profile grinding addresses as well as the rolling contact and other related surface and subsurface fatigue mechanisms, also addressed by rail grinding. However, the understanding of the grinding mechanism itself has not kept pace with the improved implementation. Thus, while railroad engineering and maintenance personnel have learned to better develop grinding patterns and profiles through empirical testing and field evaluation, the fundamental theoretical bases for the improved grinding performance have not kept pace.

One such fundamental area of understanding is the modeling of the rail grinding process itself, both individually, as a function of a single grinding motor on the head of the rail, and in the more complex configuration of multiple grinding motors in a range of patterns. At the fundamental level, grinding is performed by individual abrasive particles or grains, which are held together by a bonding material and combined to form a grinding wheel or stone. The basic grinding wheel used in the railroad industry is the 250 mm (10") grinding wheel which contains several thousand abrasive grinding grains of defined size (the grit size) , held together by a resin type bonding material. Each abrasive grain is held by bond "posts' which hold the individual grain until it is "worn out" and no longer capable of effectively cutting the rail metal. At that point the worn out grain is released to expose a fresh abrasive grain particle [1]. A production type grinding train can have 96 such grinding stones with 48 motors per rail, with each wheel (and corresponding grinding motor) operating a defined angle (which adjusts the position on the rail head) and power level. This combination of motors or patterns represents the basic approach used in modern profile grinding [2].

By understanding the grinding process from the bottom up, i.e. through initial understanding of the cutting process of individual abrasive grinding particles or grains, it is possible to better define the more global grinding process that is achieved through the application of dozens of grinding wheels, each consisting of thousands of grinding grains. In particular, it is possible to look at the key metal removal rate, that is achieved by a grinding train, from the point of view of metal removal at the individual abrasive grain level and the individual grinding wheel level (with each wheel containing thousands of individual grains).

This paper presents the results of research directly aimed at better understanding how these mechanisms interact, and in particular how the application of thousands of grinding grains results in the development of a ground rail profile. This research builds on basic cutting theory [3,4,5] and more recent research into the mechanisms of cutting and chip formation, at the individual cutting grain lavel [6,7,8,9] and applies these theories better understand the rail grinding process. This understanding is then utilized to develop a detailed rail grinding model that allows for the accurate analysis of not only an individual grinding motor but also a full grinding train application, as a function of pattern and speed.

GRINDING MECHANISMS

Basic grinding mechanism and determination of depth of cut at the abrasive grain level

The rail grinding process is the process by which a small amount of rail metal is removed from the surface of the rail head using rotary grinding motors [1]. Properly applied, this process is a "gentle" process, carefully removing a fraction of a millimeter of rail steel without introducing a rough surface finish or other surface defects in the head of the rail, which could result in defect initiation sites on their own.

As noted, this process begins at the individual grinding particle, or abrasive grain (also referred to as grit) level as it cuts into the rail head. This individual grain process is repeated thousands of time for each grinding wheel as it cuts into the rail head. Thus, it is important to understand the performance of each individual cutting grain, and in particular the basic grinding mechanism used in the rail grinding process, based on the cutting behavior of these abrasive grains. One of the critical parameters for understanding and then applying these theories of cutting and grinding is the cutting depth achieved by for individual grain. This individual grain cutting performance contains the clue to analyzing the grinding capability for the entire grinding stone and then a multi-stone (motor) grinding train. Thus, the grinding of the surface of the rail can be considered to be the summation or integration of a large number of cutting grains.

The key to determining the cutting depth achieved by each abrasive grain is the analysis of the cutting process and the resulting metal sliver or "chip" that is removed by that grain or grit. According to basic machining theory [3, 4], the cutting progress that occurs during grinding can be illustrated as shown in Figure 1. As can be seen in Figure 1, for each individual cutting grain, a chip is removed, the size of which is dependent on the geometry of the chip and the work piece (the rail). This geometry is defined by a series of three planes; the rake face (with rake angle γ), the flank face (with the flank angle α) and shear plane (with the shear angle φ). At a given cutting speed, the removed chip moves away from the rake face with a corresponding speed referred to as the chip velocity. The removed chip will have a chip thickness h_c, while the remaining portion will have the undeformed chip thickness h, which represents the cutting depth of the individual grain or grit.

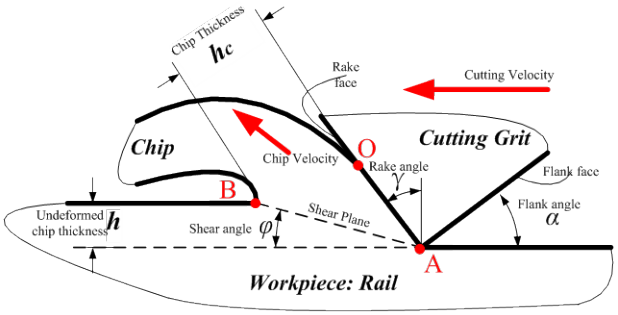

Figure 1. Schematic View of Grain and Chip Geometry

The forces involved in the cutting process have been defined by Merchant [5] based on the theory of force equilibrium. As seen in Figure 2, the removed chip is subjected to two opposing forces: T and T'. These two forces can be defined as the resultant forces at the shear plane and rake face as illustrated in Figure 2.

The force T, which the tool exerts on the chip, is resolved into the tool face-chip friction force F and normal force N. The angle β between F and N is thus the friction angle. The force T' which the workpiece exerts on the chip is resolved along the shear plane into the shearing force F_s,which is responsible for the work expended in shearing the metal , and into the normal force, F_n,which exerts compressive stress on the shear plane. Force T' is also resolved along the direction of tool motion into F_c, termed as the cutting force, and into F_t, the thrust force [5].

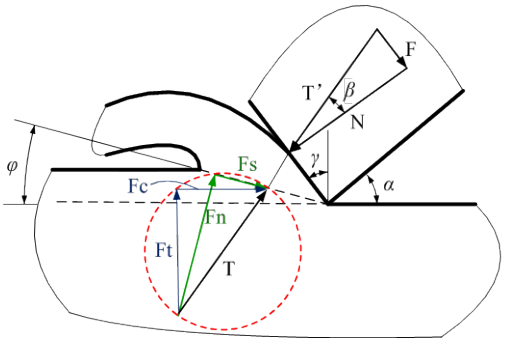

Figure 2. Force Equilibrium for Chip

The relationship between these forces can be obtained as followings:

$$\begin{cases} F_s = T\cdot\cos(\varphi+\gamma+\beta) \\ F_n = T\cdot\sin(\varphi+\gamma+\beta) \end{cases} \quad \begin{cases} F_c = T\cdot\cos(\gamma+\beta) \\ F_t = T\cdot\sin(\gamma+\beta) \end{cases} \tag{1}$$

The following analysis uses these relationships together with existing research in the area of rake cutting angles for grinding grains based on experimental studies and theoretical modeling [6~8]. Assuming that the rake angles of most of the cutting grains γ can be kept at $\gamma=60^\circ$ and that φ covers half the complementary angle of γ which means $\varphi\approx 15^\circ$, then it can be determined that

$$F_c = \frac{\cos(\gamma+\beta)}{\cos(\varphi+\gamma+\beta)} F_s \approx 2.14 F_s \tag{2}$$

The corresponding consumed cutting power can be expressed as:

$$P = F_c \cdot V_c \tag{3}$$

Where V_c is the cutting speed.

Thus, as can be seen the angles between the different component forces can be determined based on the approximate grain angles and assumed cutting depth. However, the relationships between the forces and the velocities are still not clear. Noting that the grinding train (and thus the grinding stones) is moving forward along the rail while the grinding stones are also rotating across the rail, the grains on the surfaces of the grinding stones will have a combined instantaneous speed which is a combination or resultant of the forward speed and the rotating speed. It is this resultant speed direction that will determine the chip-flow direction and also its thickness.

As shown in Figure 3, the instantaneous speed of the single cutting grain will be formed by combing the forward speed v and the rotating speed wR. In the plane of the resultant speed v_{com}, the chip will be formed with the grit thrusting into the rail. Because of the rotating effects, the instantaneous resultant speed will be changing as the grinding wheel rotates and the individual grains change location (and angle of movement) with respect to the rail surface, even though the direction of the forward speed is unchanged.

$$\begin{aligned} \overrightarrow{v_{com}} &= \vec{\omega}\times\vec{R}+\vec{v} \\ v_{com} &= \left|\overrightarrow{v_{com}}\right| = \left|\vec{\omega}\times\vec{R}+\vec{v}\right| \end{aligned} \tag{4}$$

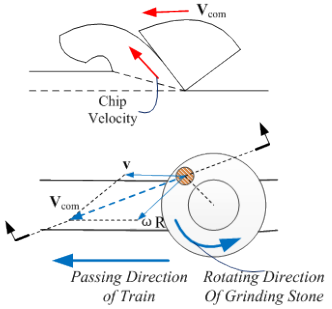

Figure 3. Chip Cutting at Combined Speed

Assuming the rotational speed of the grinding stone and the

forward speed of the grinding train are kept constant, once the position of the grain (with radius distance r to the stone center) has been determined, the instantaneous line speed can be obtained from.

$$P = \sum_{TotalGrainNo.} F_c \cdot v_{com} = Sum_{grtis} \cdot F_c \cdot v_{com} \quad (5)$$

The Power-Force-Speed model established can combine key elements in the grinding process to obtain the relationships between those factors. Thus, once the input parameters such as the grinding speed and power setting are defined, the overall grinding results, and in particular the cutting depth of the grinding, can be determined.

Thus, at the individual grinding particle level, the cutting depth for individual grains can be obtained, using the relationship between cutting force and the consumed power at the combined cutting speed v_{com} :

$$F_c = \frac{P/v_{com}}{Sum_{grtis}} \quad (6)$$

Noting that for the shear plane A_s , the shear stress τ_s and normal stress σ_s are found to be:

$$\tau_s = F_s/A_s \ , \ \tau_s \approx 0.45 \cdot \sigma_s \quad (7)$$

Then the shear plane area A_s can be defined as (see Figure 4)

$$A_s = \frac{F_s}{\tau_s} \approx \frac{F_c}{2.14\tau_s} \quad (8)$$

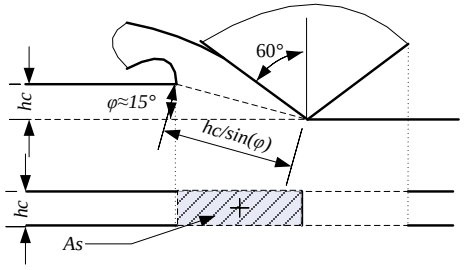

Figure 4. Geometry for Cutting Depth and Shear Plane Area

Assuming that the cutting grain has a cutting width of h_c as shown in Figure 4, and estimating the length of the shear plane to be $h_c/\sin(\varphi)$, then the area of the shear plane in Figure 4 can be computed as $A_s \approx (\sqrt{2+\sqrt{3}}/2) \cdot h_c^2$, where $h_c \approx h$ (Figure 1). The cutting depth for each individual grit h can then be determined from:

$$h = \sqrt{\frac{A_s}{\sqrt{2+\sqrt{3}}/2}} = \sqrt{\frac{F_c/2.14\tau_s}{\sqrt{2+\sqrt{3}}/2}} \quad (9)$$

$$h \approx \sqrt{\frac{F_c/\tau_s}{2.07}} \approx \sqrt{\frac{P/v_{com}}{Sum_{grtis}} \cdot \frac{1}{2.07\tau_s}} \quad (10)$$

It should be noted that the cutting depth and corresponding chip thickness will vary as a function of rail materials strength and grinding stone composition (grit size and type, wheel grade, etc. [1])

Metal removal at the Grinding Wheel Level

Once the cutting depth for the individual grains is determined, it is then possible to determine the cutting depth of a section of the surface of the rail , the grinding zone, after the passing of an individual grinding wheel (a wheel pass). It is clear the grinding process for the whole grinding wheel is more complex than simply combining a large number of grains. Given the fact that there are thousands of individual grains, moving across the surface of the rail, at a resultant speed which is related to both the rotation of the grinding stone and the forward movement of the grinding train (or in grinding terms, the movement of the workpiece- the rail), there will be many overlaps and/or untouched area on the surface of rail for the unpredicted grain locations and sizes. A schematic diagram for the distributions of grains on the surface of the grinding wheel is shown in Figure 5. Because the grains are fixed on the grinding wheel, they will change positions following the rotation of the wheel. The associated cutting tracks for these individual grains can be calculated based on the corresponding motion of the wheel and the rail (the work piece).

Defining the location of each individual grit using the radial distance to the center r_i and the angle θ_j gives..

$$\begin{cases} r_i = \dfrac{r_x}{R_{outer} - R_{inner}} \mathrm{I}_{[R_{outer}, R_{inner}]}(r_x) \\ \theta_j = \dfrac{\theta_x}{2\pi - 0} \mathrm{I}_{[0,2\pi]}(\theta_x) + \omega \cdot \mathrm{t} \end{cases} \quad \begin{cases} N_i = length(r_i) \\ N_j = length(\theta_j) \end{cases} \quad (11)$$

In addition to the rotation of the wheel, the passing speed along the rail surface will generate a displacement of the wheel center. Taking the forward direction along the rail as axis x and the transvers direction as y gives the forward speed as:

$$\begin{cases} x_c = v \cdot t \\ y_c = 0 \end{cases} \quad (12)$$

Thus the location for each grain peak ($x_{i,j}$, $y_{i,j}$) can be determined (see Figure 5) with respect to the coordinates for the wheel center at any time t:

$$\begin{cases} x_{i,j} = x_c + r_i \cdot \cos(\theta_j) & i \in (1, 2, \cdots, N_i) \\ y_{i,j} = y_c + r_i \cdot \sin(\theta_j) & j \in (1, 2, \cdots, N_j) \end{cases} \quad (13)$$

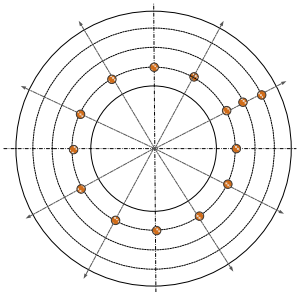

Figure 5. Schematic Diagram for Grit Distribution

As the cutting grains penetrate into the rail surface, the z direction, there will be interaction between the grain cutting peaks and the rail surface. This, in turn generates a three-dimensional set of results by combining the grains locations, the cutting depth h and the cutting width h_w. Based on the grinding mechanism above, the grain shape at the cutting plane has been assumed to be a triangle which peaks into the rail surface as illustrated in Figures 6 and 7.

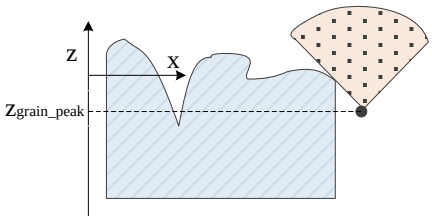

(a) Before grinding

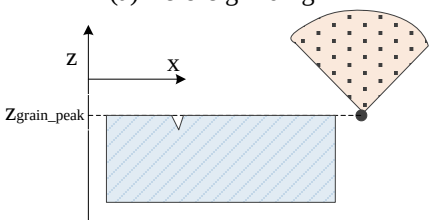

(b) After Grinding

Figure 6. Comparison of z value with Grain_peak and Surface to be Ground

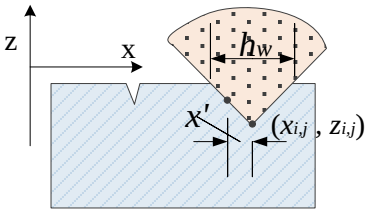

Figure 7. Coordinate Value for Points Around Cutting Peak

As shown in Figure 7, locations (coordinates) for points at and around the cutting peaks can be then be estimated as:

$$z_{grain\_peak}^{i,j} = -h$$
$$z_{grain\_around}^{i,j} = -h + \frac{x' - x_{i,j}}{h_w} h \qquad (14)$$

Where x' represents the points at the cutting edges around peaks.

The ground surface will be calculated as:

$$z_{i,j} = \min(z_{grain}^{i,j}, z_{rail}^{i,j}) \qquad (15)$$

Which means that the valleys on the surface lower than the cutting peaks cannot be touched by the cutting grains.
The grinding depth for each area will then be calculated from:

$$D = \frac{V_{area}}{Area} = \frac{\sum z_{i,j} \cdot Area_{i,j}}{Area} \qquad (16)$$

Equation (16) is then used to calculate the average grinding depth for a defined area with an appropriate number of cutting points. Thus for example, a $1\text{mm} \times 1\text{mm}$ square zone is defined with 1000×1000 points. Thus for each point, $Area_{i,j} = 0.001\text{mm} \times 0.001\text{mm}$. Using the z values for each cutting point (Figure 7), based on the location of each passing grinding grain (cutting point), the change in surface volume can be calculating using $\sum z_{i,j} \cdot Area_{i,j}$ which represents the "volume" of metal removal for the zone (assuming z=0 for all points before grinding). The average depth D can then be calculated as noted above.

COMPARISON WITH TEST DATA

Comparison with Grinding Wheel Data

In order to illustrate this behavior, data from proprietary grinding wheel tests [1] have been used to compare the theoretical analysis of grinding with the actual test data, representing a single grinding wheel moving along a slowly rotating work piece representing the rail.

These single wheel tests have been implemented using the same type of grinding wheels used in production rail grinding (and as such will also be compared with the full train grinding results discussed later in this paper). Furthermore, the work piece used in the grinding tests has similar material properties as rail.

The test parameters for the single grinding wheel test are presented in Table1. Note, the forward travelling motion of the grinding train has been simulated by the circular motion of the work piece.

[1] Permission has been given to show only limited average results, which are presented here-in.

Table 1. Parameters for Test

Parameters	Value
Grinding Wheel Outer Diameter (mm)	250
Grinding Wheel Inner Diameter (mm)	150
Grinding Wheel Rotation Speed (rpm)	3629
Workpiece Outer Diameter (mm)	1211
Workpiece Inner Diameter	1192
Workpiece Rotation Speed (rpm)	28
Workpiece Surface Speed (m/s)	1.75
Table Infeed Rate (mm/rev)	0.33

Using these parameters in the theoretical model, the average cutting depth for individual grains is calculated. Using the theory of the individual grinding grain cut, and the additional theory of the wheel behavior, as presented here, the ground surface for the each specific topography zone (rail surface area) can be computed based on the motion of each effective grain.

Because of the proprietary nature of the grinding stones, actual data on the grain size, grade, number of grains, etc. was not available and was estimated based on industry data [1]. Likewise, the data on the workpiece was estimated based on the properties of standard carbon railroad rail. These estimated properties are presented in Table 2. In order to save computing time, only a small zone, the topography zone, has been used in the calculation to represent the effects of a single grinding wheel pass.

Table 2. Parameters for Calculation

Parameters	Values
Grinding Wheel Outer Diameter (mm)	250
Grinding Wheel Inner Diameter (mm)	150
Grit Size (um)	500
Estimated Instantaneous Grain No. Sum_{grits}	2×10^3
Tensile Strength σ_s (N/mm^2)	780
Shear Strength $\tau_s \approx 0.45\cdot\sigma_s$ (N/mm^2)	351
Grinding Wheel Rotation (rpm)	3629
Cutting Speed $v_{com}=\left\vert\vec{\omega}\times\vec{R}+\vec{v}\right\vert$ (m/s)	38
Passing Speed (m/s)	1.75
Equivalent Feed Rate on Wheel(mm/rev)	0.0025
Topography Zone ($\text{mm}\times\text{mm}$)	1×1

It should again be noted that in a single grinding pass of the workpiece (the rail), multiple cuts are obtained for each grinding particle and the resulting metal removal on the work piece (the rail) is illustrated by the topographical representation shown in Figure 8.

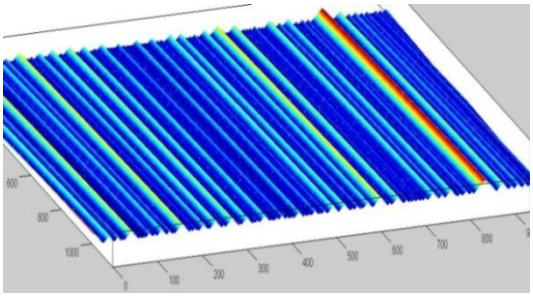

Figure 8. Topography Graph on Chosen Zone

The overall cutting depth for this zone can be then calculated and compared with the average measured depth of cut from the test. This is shown in Table 3 based on the equation for cutting depth of individual grit

$$h \approx \sqrt{\frac{P/v_{com}}{Sum_{grtis}} \cdot \frac{1}{2.07\tau_s}}$$

Table 3. Comparison with Test & Simulation

Grinding Power P (KW)	Measured Cut Depth (mm)	Cutting Depth Of Grain (um)	Cal'd Cut Depth (mm)
37.66	0.2160	24.5	0.2080
32.44	0.1727	21.0	0.1800
24.24	0.0935	18.1	0.1551

As can be seen in Table3, the measured depth of cut, from the test, and the calculated depth of cut, from the grinding theory show good agreement for the higher horsepower levels and moderate agreement with the lower horsepower level. Note there is a clear relationship between depth of cut and horsepower. A possible explanation for the shallower depth of cut for the lower horsepower is that at lower power settings, the grinding wheel is cutting at a less than optimum efficiency for the stone configuration (e.g. grade, grit type and size, etc.). This is supported by the grinding literature which suggests that the metal removal- power relationship varies as a function of wheel grade [1].

It should be also noted that based on the cutting depth of each grain and the total cutting depth, approximately 8.5 cuts are made per single grinding pass (on the rail).

Metal Removal at the Grinding Train Level

In order to move from the grinding wheel level to the grinding train level, it is necessary to combine multiple wheels, with each wheel operating at a different motor angle (and as a result a different position on the top of the rail, with a different surface radius) and possibly different power settings. This combination of grinding motors and power settings is referred to as a pattern, with corresponding different metal removal behavior associated with each pattern.

The traditional approach to analysis of metal removal as a function of grinding pattern (size of grinding train, number of motors, horsepower, speed, etc.) is to assume a constant volume of metal removal per unit time Q, usually defined in cubic inches per minute or cubic mm per minute. This value can be obtained from grinding tests such as discussed previously or from calculation of the total volume of metal removal per grinding pass of a train (taking into account speed of the train and number of working motors). Thus for example, the tests discussed in Table 3 had a Q of approximately 1500 cubic mm per second at approximately 22 KW (5.57 cubic inches per minute at 30 HP).

By assuming constant volume per motor (and at a constant grinding speed, constant cross-sectional area of metal removal per motor), and assuming a contact geometry directly related to the local radius on the rail head, the corresponding metal removal per pattern can be calculated [8]. This is illustrated in Figure 5 through 7.

Figure 9 shows the individual grinding wheel position across the rail head as a function of motor angle. As can be seen, grinding wheels with different angles will have different contact points with the rail head and corresponding different rail head radii at the point of wheel contact.. This directly relates to the wheel contact length (and associated width of the grinding facet) and thus to the cutting depth, which will vary accordingly.

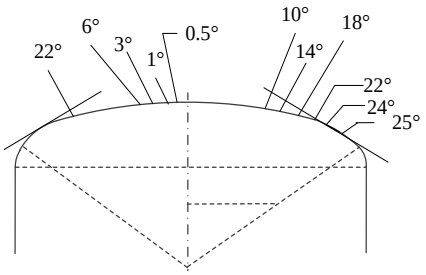

Figure 9. Transversal Angle Distribution of Grinding Wheels [1]

The relationship between grinding angles and cutting depths can be obtained based on the actual rail profile (such as from a digital profile measurement system [10, 11]), the contact width of the stone and the rail head, and the 'constant" area of metal removal (constant for a given grinding or forward speed). Given the fact that the width of the cut will vary as a function of the depth of penetration, as seen in Figure 10, most models calculate the cutting process in a step by step manner until the area of metal removal is obtained [9]. This in turn yields the depth of cut per motor.

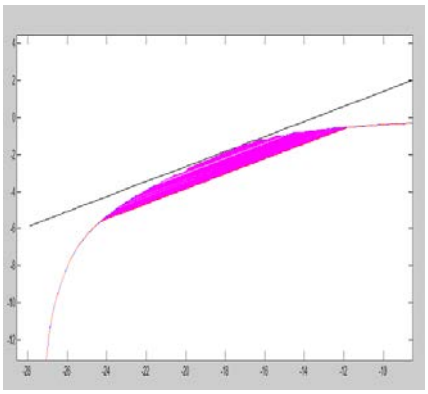

Figure 10. Cutting into Rail head Step-by-Step

This is repeated for each of the grinding motors in the pattern, with a corresponding motor angle and rail head position for each motor. Furthermore, the cutting sequence has a significant effect on the metal removal and on the ground rail profile. This is because the first grinding wheel will make its initial cut, changing the rail profile that the second motor sees, and thus the second motor must address the 'cut' profile. This is illustrated in Figure 11, which shows how the contact point of the second motor will differ if it follows the first motor or if it is on the rail where no previous cut has occurred. Note the displacement of the contact point in Figure 11.

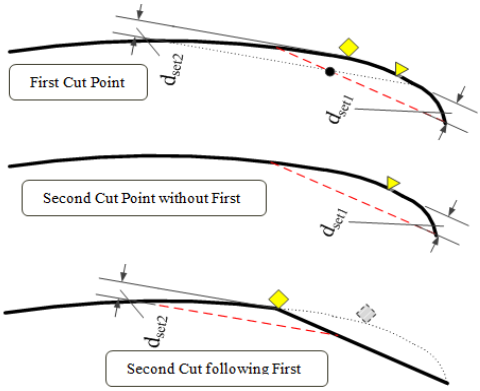

Figure 11. Cutting Sequence Effects

When this is applied to a full grinding pattern, such as with a 96 motor train with 48 motors per rail, the resulting calculation must take this sequence effect into account, usually as part of the programming process which includes the full set of grinding wheels with different setting angles and powers [8]. Tables 4 and 5 illustrate two such sets of grinding patterns.

Table4. Setting Angles and Powers of Pattern01

Angle	-1	-3	-7	3	7	12	14	-11	18	20	25	28	30	23	14	12	-15	10	15	-6	-8	5	1	0
Motor No.	1	3	5	7	9	11	13	15	17	19	21	23	25	27	29	31	33	35	37	39	41	43	45	47
	|	|	|	|	|	|	|	|	|	|	|	|	|	|	|	|	|	|	|	|	|	|	|	|
	2	4	6	8	10	12	14	16	18	20	22	24	26	28	30	32	34	36	38	40	42	44	46	48
Hp	23	23	23	23	23	21	21	22	20	20	19	19	19	19	21	21	21	23	21	23	23	23	23	23

Table5. Setting Angles and Powers of Pattern02

Angle	-1	-3	-7	3	7	12	14	-11	18	20	25	28	30	23	14	12	-15	10	15	-6	-8	5	1	0
Motor No.	1	3	5	7	9	11	13	15	17	19	21	23	25	27	29	31	33	35	37	39	41	43	45	47
	|	|	|	|	|	|	|	|	|	|	|	|	|	|	|	|	|	|	|	|	|	|	|	|
	2	4	6	8	10	12	14	16	18	20	22	24	26	28	30	32	34	36	38	40	42	44	46	48
Hp	19	19	19	19	19	19	20	21	21	21	22	22	23	23	23	23	23	23	23	23	22	22	21	23

Detailed metal removal field data was available from a series of field tests conducted by Harsco Rail on a US Class 1 railroad as reported in references 9 and 10. Results from 10 different measurement sites[2] (5 each for two different sets of grinding patterns) are presented respectively in Table 6 and Table 7 and compared to both the individual grinding wheel test results and the grinding theory which is built up from the individual cutting grain level. While there is some uncertainty as to the actual power setting of the grinding train, preliminary comparison of the grinding train per stone metal removal rates and the grinding wheel tests show good agreement.

[2] Each site corresponds to a detailed 'before" and "after" grinding set of measurements at the exact same location as discussed in References 9 and 10.

Table 6. Removal Rate Comparison for Grinding Train Pattern 01, Tests and Theory

Grinding Train Measurement	Curve[3]	Speed (mph)	Pattern	Area Removal in^2	Area_perStone (10^{-3} in^2)	Q_field/Stone in^3/min	Q_Test[4] in^3/min	Q_Cal'd in^3/min
1	2.00	8	01	0.031	0.6458	5.4560	5.5677	4.7020
2	1.00	8	01	0.032	0.6667	5.6320	5.5677	4.5771
3	1.00	8	01	0.016	0.3333	2.8160	5.5677	4.5779
4	1.00	8	01	0.031	0.6458	5.4560	5.5677	4.7020
5	2.45	8	01	0.029	0.6042	5.1040	5.5677	4.5171
Average 4.89	5.57	4.62						

Table 7. Removal Rate Comparison for Grinding Train Pattern 02, Wheel and Theory

Grinding Train Measurement	Curve	Speed (mph)	Pattern	Area Removal (in^2)	Area_perStone (10^{-3} in^2)	Q_field/Stone in^3/min	Q_Test**Error ! Bookmark not defined.** in^3/min	Q_Cal'd in^3/min
1	1.2	8	02	0.020	0.4167	3.5200	5.5677	4.5277
2	4.4	8	02	0.031	0.6458	5.4560	5.5677	4.1081
3	5	8	02	0.009	0.1875	1.5840	5.5677	3.9690
4	1	8	02	0.023	0.4792	4.0480	5.5677	4.2172
5	4	8	02	0.017	0.3542	2.9920	5.5677	4.1770
Average						3.52	5.57	4.20

In the case of Table 6 (pattern 01) , the average Q for the five field measurements was 4.89 cubic inches per minute as compared to a Q of 5.57 cubic inches per minute for the wheel test. The average calculated Q (from cutting grain theory) was 4.62 cubic inches per minute. In the case of Table 7 (pattern 02) , the average Q for the five field measurements was 3.52 cubic inches per minute as compared to a Q of 5.57 cubic inches per minute for the wheel test. The average calculated Q (from cutting grain theory) was 4.2 cubic inches per minute.

While the variation between the three different analyses/tests was greater in Table 7 (pattern 02) than in Table 6 (pattern 1), the results are still reasonable. Figures 12a and 12b present this data graphically. Again it is noted that the actual power settings for the full train metal removal data, which shows the greatest variation from measurement to measurement, are not know and were assumed to be at the "normal" grinding setting for the patterns. The power settings for the wheel tests and the grinding theory are better defined (Table 3).

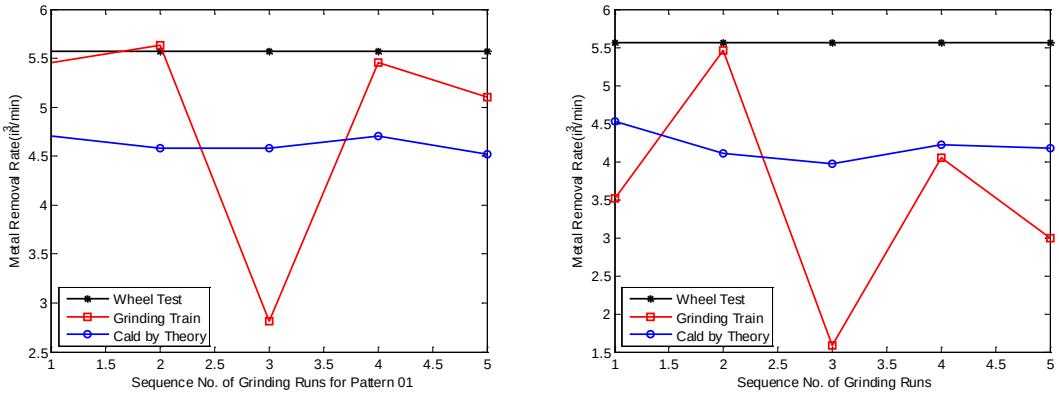

(a) (b)

Figure 12. Removal Rate Comparison Between field tests, Wheel Test and Theory

[3] Track Curvature in degrees of curvature D (D = 5730/R, where R = radius of curvature in feet)

[4] Average of multiple grinding tests

Specifically, Figure 12 presents the data from Tables 6 and 7 graphically for each of the five grinding measurements (runs) in each pattern. The black star-line represents the average metal removal rate from the single grinding wheel tests. The red square-line represents the metal removal rate obtained from measurement of the grinding train runs. The blue circle-line represents the metal removal rate from the cutting grain theory, using the same rail profiles as used with the respective runs of grinding train.

As noted previously, the metal removal rates are constant for the wheel test (based on an average of three tests with only modest variation in the results between tests) and are quite similar for the grinding theory (with the variation due primarily to the differences in profile of the rail head which differed from run to run) . However, the variation in metal removal rates is significantly greater for the five grinding runs, which suggests that there are differences in the individual grinding runs which may include variation in the actual power levels that were used, differences in rail hardness and profile, curvature effects, and other operating conditions not noted in the specific grinding report (note speed and pattern were constant for each set and curvature was reasonable similar). In addition, dynamics in the grinding process itself, perhaps at the grinding wheel/rail interface, may have significant effects on the variability of the grinding results.

In spite of these variations, as noted previously, the agreement between the three methods in the case of pattern 01 was quite good and even for pattern 02 the results are still reasonable. Furthermore, noting the general agreement of the analysis with the data, it is believed that with improved detailed grinding information and corresponding estimation of the specific parameters in the grinding process, the theoretical calculation will be closer to the field data. This in turn will provide a more powerful tool to evaluate future grinding patterns.

SUMMARY

This paper presents a bottoms up approach to rail grinding theory, using basic cutting theory, in the form of individual abrasive particles or grains and then combining them at the wheel level to look at metal removal (and depth of cut) per wheel. This is in turn further combined at the grinding train level to look at how the basic grinding theory compares with actual field results from a full scale large production grinding train.

The paper shows that it is possible to model the rail grinding process itself, at the grinding grain level, and then build up the process to look at a single grinding motor on the head of the rail, and finally in the more complex configuration of multiple grinding motors in a range of patterns. The fundamental theory addresses how grinding is performed by individual abrasive particles or grains, and how they generate a metal chip (and the associated depth of cut). Combining several thousand of these grains into a standard industry 250 mm (10”) grinding wheel requires understanding of the relative motion of the rotating wheel and the forward speed for the train since for each pass of the wheel on the rail, multiple cuts are made by each particle.

Further combining these into the grinding train level requires incorporation of the individual motor angle and power settings designed into a full grinding pattern.

By understanding the grinding process from the bottom up, i.e. through initial understanding of the cutting process of individual abrasive grinding particles or grains, it is possible to better define the more global grinding process that is achieved through the application of dozens of grinding wheels, each consisting of thousands of grinding grains. In particular, it is possible to look at the key metal removal rate, that is achieved by a grinding train, from the point of view of metal removal at the individual abrasive grain level and the individual grinding wheel level (with each wheel containing thousands of individual grains). This is shown in the results which indicates reasonably good agreement between the theory and the single wheel test as well as in the full scale grinding data which shows modest agreement (with significant variation in the field grinding data itself).

By better understanding how these mechanisms interact, and in particular how the application of thousands of grinding grains results in the development of a ground rail profile, better models can be developed to allow for the accurate analysis of existing and new grinding patterns in a full grinding train application, as a function of pattern and speed. This in turn will allow for improved optimization of the actual grinding process in the field and the developed of optimized grinding strategies.

ACKNOWLEDGEMENT

The authors would like to acknowledge Harsco Rail for contributing to the funding of this research.

REFERENCES

1. Zarembski, A.M., The Art and Science of Rail Grinding, **Simmons-Boardman Books, Inc.,** Omaha, NE, August 2005
2. Zarembski, A.M., "Management of Total Rail Grinding Maintenance Process", **Railway Track & Structures**, June 2011
3. Marinescu, I. D., Rowe, W. B., Dimitrov, B and Inasaki, I, Tribology of Abrasive Machining Processes, William Andrew Publishing, Norwich, NY 2004
4. DeVries, W. R., Analysis of Material Removal Processes, Springer-Verlag, NY 1992
5. Merchant, Mechanics of the Metal Cutting Process, ii: Plasticity Conditions in Orthogonal Cutting, Journal of Applied Physics, 1945,16: 318-324.
6. Huang, Y.; Liang, S. Y., Force modeling in shallow cuts with large negative rake angle and large nose radius tools—application to hard turning, International Journal of Advanced Manufacturing Technology, 2003, (22): 626-632
7. Vinogradov, A. A., On Chip Formation in Cutting Metallic Materials Using Tools with a Large Negative Rake, Journal of Superhard Materials, 2011, 4(33): 255-260
8. Ohbuchi, Y.; Obikawa, T., Finite Element Modeling of Chip Formation in the Domain of Rake Angle Cutting, Transactions of the ASME, 2003, 125: 324-332
9. Zarembski, A. M. and Zhi, S.D. ,"Analyzing Rail Grinding Patterns", Railway Track & Structures, June 2013.
10. Zarembski, A.M., "High Speed Rail Grinding for High Speed Rail", **7th World Congress on High Speed Rail**, Beijing, China, December 2010.
11. Zarembski, A.M., Hagan, B., "Effectiveness of High Speed Rail Grinding on Metal Removal and Grinding Productivity", 2011 **AREMA Annual Conference**, Minneapolis, MN September 2011.